C,N-doped TiO2 monoliths with hierarchical macro-/mesoporosity for water treatment under visible light

Paolo Boscaro, Thomas Cacciaguerra, Didier Cot, François Fajula, Vasile Null Hulea, Anne Galarneau

C,N-doped TiO_2 monoliths with hierarchical macro-/mesoporosity for water treatment under visible light

Paolo Boscaro [a], Thomas Cacciaguerra [a], Didier Cot [b], Francois Fajula [a], Vasile Hulea [a], Anne Galarneau [a] *

[a] Institut Charles Gerhardt Montpellier, UMR 5253 CNRS - Univ Montpellier - ENSCM, ENSCM, 240 avenue du Professeur Emile Jeanbrau, 34 296 Montpellier Cedex 5, France.

[b] IEM (Institu Europeen des Membranes), UMR 5635 CNRS - Univ Montpellier - ENSCM, Univ Montpellier, 2 Place E. Bataillon, 34 095 Montpellier, France.

*Corresponding author: E-mail address: anne.galarneau@enscm.fr (A. Galarneau)

ABSTRACT: C,N-TiO_2 monoliths with homogeneous interconnected macro-/mesoporous hierarchical porosity, consisting in 83% anatase phase, exhibiting high visible light absorption were prepared in one pot synthesis. The hierarchical porosity was controlled by coupling a sol-gel method with a spinodal decomposition and the improved visible light absorption was obtained by self C,N-grafting during thermal treatment. Titanium isopropoxide, N-methylformamide, poly(ethylene oxide), and hydrochloric acid were used as reagents to form a sol, which was then treated at 40 and 60 °C, followed by a solvothermal treatment in autoclave at 200°C in isopropanol. The monoliths were further heated at different temperatures from 250 to 500 °C under air. The best compromise between the structural and textural properties (TiO_2 phase, surface, volume, pore diameter), the visible light absorbance and the mechanical properties was obtained for a calcination at 350°C for 5 hours. In batch mode, in glass containers, the monoliths demonstrated remarkable efficiency as photocatalysts under natural sunlight and artificial visible light for the degradation of the azo dye Orange G in water compared to benchmark TiO_2 P25 nanoparticles, which proved inefficient under these conditions. More interestingly, the monoliths used as reactors in flow mode in a recirculating system proved very efficient for the total elimination of Orange G dye revealing the high potential of these TiO_2 monoliths for continuous flow wastewater treatment under visible light.

KEYWORDS: TiO_2 monolith; visible light; photocatalysis; dyes degradation; flow process; wastewater treatment.

1. Introduction

In the last ten years our group studied silica, titania and zeolite monolithic materials with hierarchical porosity (macro-/mesoporosity) and their applications in heterogeneous catalysis and in adsorption in continuous flow reactors [1-3]. High catalytic and adsorption performances have been obtained with these monoliths due to optimal fluid dynamics within the interconnected network of pores. To extend the applications of the monoliths to photocatalysis under continuous flow conditions, and possibly under visible light, we prepared hierarchical macro-/mesoporous C,N-self-grafted TiO_2 monoliths featuring high mechanically stability and high visible light absorption.

Pure, non-doped, TiO_2 is an efficient photocatalyst [4-10], but it shows some shortcomings. Among them, the wide band gap of anatase (3.2 eV), which restrains its use essentially to UV light. From a practical and environmental point of view, it is crucial to develop visible-light active TiO_2 by decreasing gap energy. The strategies adopted to enhance the photocatalytic efficiency of TiO_2 materials include either morphological/textural changes (tailoring the surface size/complexity, crystalline phase, pore and particle size), or chemical modification by incorporation of additional components in the TiO_2 structure (doping with organic and inorganic species) [11-14].

The most frequent chemical modifications of the TiO_2 lattice involve doping with elements like B, N, F, C, P, Cl, Br and S. Nitrogen and carbon, offer the most appropriated results in term of photocatalytic activity and easiness of utilization [15-21]. TiO_2 can be doped with one element (C, N) [22] or co-doped with both elements [23-25]. According to literature data, by doping, the E atoms (E = N, C) are able to substitute lattice oxygen atoms in the TiO_2 network and form Ti-E or O-Ti-E arrangements [26,27]. The new bonds produce hybrid orbitals just above the valence band of TiO_2 and bestow enhanced visible light absorbance [28].

Most photocatalytic applications use TiO_2 nanoparticles/nanopowders with well-defined size and high crystallinity. The most used material in photocatalysis is TiO_2 P25 (obtained from Degussa or Evonik Industries) featuring nanoparticles of 20 nm composed of 80% anatase and 20 % rutile and a specific surface area of 50 m^2/g. This material often used

as a benchmark features high efficiency in photocatalysis under UV light (higher efficiency with UV-C in comparison to UV-A). Typically, TiO_2 nanoparticles with diameters of 5–50 nm are highly efficient photocatalysts due to their elevated surface area and numerous active sites, in comparison to their larger particle diameters counterparts. Moreover, by reducing particle size at the nanometric length scale, the band gap and the position of the valence and conducting bands in TiO_2 are strongly modified, with possible beneficial effect on the photocatalytic activity [29,30]. However, the use of TiO_2 nanoparticles is still limited, because, nanoparticles are subjected to agglomeration, and moreover the removal of the TiO_2 nanoparticles powder suspended in the treated systems is a very difficult task. Additionally, TiO_2 is likely to encounter greater mass transfer limitation for the associated surface mediated reactions involving organic contaminants in water [31].

The introduction of controlled porosity in TiO_2 based materials is a promising mean for improving the textural and diffusion properties and the overall photocatalytic activity. Common methods used for preparing porous TiO_2 materials uses removable or sacrificial templates, including soft templating (surfactant micelles, bi- or tri-block copolymers, ionic liquids) [32,33] and hard templating (silica, colloidal crystals, polymeric beads) [34,35] approaches. In order to overcome other drawbacks of the TiO_2 nanoparticles, such as agglomeration, separation and powders removal after use, configurations with nanoparticles being incorporated on a support [36-39], or immobilized on monoliths with interconnected macropores have been proposed [40]. Efficient results in photocatalysis under UV lights have been obtained with the deposition of P25 on SiC foams, but only few amount of TiO_2 could be deposited on the supports and SiC foams, which are also quite fragile [40]. New kinds of monoliths, more robust, have to be found.

Yu et al. [41] reported sponge-like macro-/mesoporous TiO_2 powder (anatase phase) prepared from titanium tetrabutoxide without using templates or additives at room temperature, followed by thermal treatment. The materials present macropores of 2-4 μm parallel to each other and perpendicular to the outer surface of the particles with pore-wall thicknesses of 1-2 μm. The calcination temperature appeared to be critical for photocatalytic applications as the thermal stability of the mesoporous is the key for high efficiency. The study clearly illustrated the higher efficiency of TiO_2 materials with a hierarchical macro-/mesoporosity together with high surface area. However, as for P25, these materials are under powder form, which is not a suitable shape for continuous flow applications. Konishi et al. [42,43] prepared macro-/mesoporous TiO_2 monoliths by spinodal decomposition for use in chromatographic applications. Materials were prepared according to a sol–gel process using

titanium n-propoxide as source of titanium ($Ti(O^nPr)_4$), poly(ethylene oxide) as a phase separator and N-methylformamide as a proton scavenger. Heat treatment induced the formation of an interconnected TiO_2 macro-/mesoporous framework with mesoporous structures arising from pores in between aggregated nanoparticles. This kind of macro-/mesoporous TiO_2 monolith (slightly modified method) was used successfully in selective hydrogenation of alkynes in continuous flow after Pd nanoparticles fonctionnalization [1].

In the present work meso/macroporous C,N co-doped TiO_2 monoliths were prepared using titanium isopropoxide, polyethylene oxide (PEO 20 kDa), HCl (37%) and N-methylformamide (NMF) through combined sol-gel and spinodal phase separation chemistries [3]. An additional solvothermal treatment in isopropanol was used to increase the stability of the tubular monoliths. The potential of C,N-TiO_2 monoliths as microreactors for the degradation of organic compounds contained in wastewater was evaluated in continuous flow mode under visible light using the azo dye Orange G as model solute.

2. Materials and methods

2.1. Chemicals

Titanium(IV) isopropoxide ($Ti(O^iPr)_4$, 97%, Sigma Aldrich), N-methylformamide (NMF, 99%, Sigma Aldrich), hydrochloric acid (HCl, 37%, Sigma Aldrich), and poly(ethylene oxide) (PEO, BioUltra, Sigma Aldrich) with molecular weight 20 kDa were used as received. Distilled water with a resistivity of about 15 mΩ/mm was used. The azo dye sodium,7-oxo-8-(phenylhydrazinylidene) naphthalene-1,3-disulfonic acid (known as Orange G) purchased by Certistain, was used as model molecule for the photocatalytic measurements.

Tubular molds in PVC were used to give the shape to the monolith during the first step synthesis sealed with Parafilm M.

Transparent heat shrinkable gains (ref. GFEB1/4 1.6) of 6.4 mm internal diameter in FluoroEthylenePropylene (FEP 1/4" 1.6) have been purchased from Castello France, with size in accordance with the diameter of the monoliths and the junction with the glass tubes (6 mm) assuring the connection to the HPLC pump. The monolith and the two ended glass tubes have been introduced into the gain and heat at 180° C for 2 h to form the reactor.

2.2. Photocatalyst preparation

The TiO_2-based materials were prepared following the steps depicted in Figure 1. In the synthesis, 11.2 g of $Ti(O^iPr)_4$ (97%) were placed inside a flask into a freezer at -19 °C until freezing. PEO 20 kDa, HCl (37%) and NMF were kept at 0 °C into an ice bath. Once reagents reached the temperature, the flask containing Ti alkoxide was placed into the ice-bath and stirred with a magnetic stirrer at 50 rpm. 1.75 mL HCl (37%) were added slowly under stirring and stirring rate was gradually raised to 400 rpm until getting a transparent solution. 0.361 g PEO were then added and stirred 2-3 minutes until obtaining a clear solution. Then 2 mL NMF were added under vigorous stirring (500-600 rpm) for ca. 10 min until obtaining a clear solution. The molar ratio of the resulting mixture was: 1 Ti / 0.885 NMF / 0.2144 EO / 0.5524 HCl / 1.904 H_2O; EO meaning moles of ethylene oxide groups (CH_2CH_2O). The amount of PEO is very important, without PEO no gelation occurs. The solution is then transferred into cylindrical PVC molds kept previously at 0 °C (PVC tubes of 8 mm diameter and 10 cm length) ended by PVC caps. Tubes were sealed with parafilm and placed into a 5 L glass beaker water bath at 40 °C for 24 h (gelation step). After gelation, tubes were transferred into an identical water bath, at 60 °C for 24 h (condensation period). After condensation, tubes were opened and the light-yellow monoliths were easily recovered from the tubes due to monoliths shrinkage (6 mm diameter) and placed in the bottom of a large autoclave and covered with isopropanol and heated at 200 °C for 24 h. The monoliths were then dried at room temperature for one day and at 40 °C for 10 h. The monoliths were then heated under air in a carbolite muffle, on ceramic sample holder, with a heating rate of 0.5 °C/min up to a final temperature between 250 and 500 °C, which was maintained for 5 hours.

2.3. Photocatalyst characterisation techniques

The chemical composition of the materials was determined by elemental analyses using the X-Ray Fluorescence method at Institut des Sciences Analytiques UMR 5280 CNRS Villeurbanne, France. EDS chemical analysis were performed on a FEI Quanta 200F (15 kV) apparatus PT MEA. The phases (brookite, anatase, rutile) [44] identification of the calcined TiO_2 monoliths was carried out by XRD on a Bruker AXS D8 diffractometer, using Cu Kα radiation and a Ni filter. The samples were scanned from $2\theta = 2$ to 70° in steps of 0.02°. The percentage of each crystalline phase was done with the EVA FPM Evaluation ICDD's data base.

The textural characterization of the monoliths was achieved on monoliths pieces by using nitrogen gas adsorption/desorption method at -196 °C on a Micrometrics ASAP 2020

automatic analyzer. The samples were previously outgassed under vacuum at 250 °C for 12 h. The specific surface areas S_{BET} were calculated in the domain of validity of the BET equation [3]. The pore diameters were evaluated from the nitrogen desorption isotherms using the Broekhoff and de Boer method as it is considered as one of the most accurate methods for mesopore diameter determination as demonstrated in the case of ordered mesoporous silica [45].

Diffuse reflectance UV–Vis (DRUV–Vis) spectra were recorded under ambient conditions on a PerkinElmer Lambda 14 spectrometer equipped with a $BaSO_4$ coated integration sphere; the samples were diluted in $BaSO_4$; the spectra were plotted using the Kubelka–Munk function.

Monolith morphology was studied using a Hitachi S-4800 I Scanning Electron Microscope (SEM).

X-ray photoelectron spectroscopy (XPS) measurements were performed on an ESCALAB 250 (Thermo Electron) spectrometer equipped with an Al Kα source (1486.6 eV). The surface analyzed, on which a film of Au was deposited, had a diameter of 400 µm. Spectra were calibrated with the C1s C-C bond peak at 284,8 eV.

Thermogravimetric analyses (TGA) have been performed using a Netzsch Iris TG 209C apparatus. Experiments were carried out under a flow of dry air (20 mL/min), from 35 to 900 °C, with a heating rate of 10°C/min.

2.4. Photocatalytic experiments

The photocatalytic activity of the materials has been evaluated through a set of experiments, in batch and flow modes, under either artificial or natural sunlight using pyrex glass vessel reactors.

A first series of experiments were conducted in batch to compare the activity of C,N-TiO_2 monoliths to that of benchmarck P25 TiO_2 nanoparticles under natural sunlight. Monolith pieces (1 g) were placed in three 60 mL closed containers, one wrapped in aluminium foil and maintained in the dark far from heat sources for 10 h to analyze the adsorption properties of the materials while the two other pieces (prepared from two different synthesis batches) were exposed to sunlight (Montpellier, France, South orientation, irradiation: 3.86 kWh/m² in March) from 9 am to 7 pm. The flasks were filled with 40 mL of Orange G solution (80 mg/L), corresponding to 25 g/L of material, and stirred with a magnetic stirrer. Two additional flasks were filled with the same solution and exposed the same way to sunlight, one containing 1 g of P25 TiO_2 nanoparticles and one flask free of any

photocatalyst. The discoloration of the solutions was followed as a function of time (after 1, 5 and 10 h) by sampling aliquots of the supernatant and recording after filtration the UV-Vis spectra of the solution in the domain 250 – 500 nm to calculate the remaining Orange G concentration. Orange G features two main peaks, one centered at 325 nm and a double intense peak around 490 nm. The concentration of the remaining Orange G was calculated from the intensity of the signal between 480 and 495 nm using the Beer-Lambert law.

A second comparative test with P25 TiO_2 was performed under visible light provided by a neon lamp (UVP-HPK125, Ne Pen-Ray). In order to limit a possible influence of particle size and texture, 0.147 mg of crushed C,N-TiO_2 monolith and of P25 were shaped as pellets (2.5 cm^2) by packing under a pressure of 14-17 kN/cm^2. The pellets were placed in 20 mL (7.35 g/L) of Orange G solution (80 mg/L) and exposed to visible light with for 90 minutes without stirring to avoid pellets breaking.

The degradation of Orange G under continuous flow mode has been investigated in a recirculating system with a C,N-TiO_2 monolith of 6 mm diameter and 1.4 cm length (0.366 g). The monolith has been cladded with a transparent FEP heat shrinkable gain ended by two glass tubes to insure the connections with the peristatic HPLC pump through swageloks. To eliminate the contribution of adsorption, the cladded monolith was previously soaked into an Orange G solution (80 mg/L) for 1 day without light exposition. A 50 mL solution of Orange G (80 mg/L) has been recirculated through the monolith at a flow rate of 2 mL/min under sunlight. Periodically, samples of 1 mL were collected and analyzed by UV spectroscopy.

3. Results and discussion

3.1. Textural and structural characteristics of TiO_2 monoliths

The influence of the thermal treatment on the prepared TiO_2 monolith was studied applying a slow rate of temperature increase of 0.5 °C/min. XRD patterns of samples calcined at different temperatures between 250 and 550 °C are shown in Figure 2a. These diffractograms reveal the presence of 3 crystalline phases of TiO_2: brookite, anatase and rutile. Among them rutile and anatase phases are most commonly used in photocatalysis. Both of them have a tetragonal structure. Rutile is a high-temperature stable phase and has an optical energy band of 3.0 eV (415 nm) and anatase is formed at lower temperature with an optical energy band gap of 3.2 eV (380 nm). The strong diffraction peaks of the C,N-TiO_2 monoliths (Fig. 2a) at 25° (101) and 48° (200) indicated TiO_2 in anatase phase. The peaks at

27° (110), 36° (101) and 55° (211) indicated TiO_2 in rutile phase. The percentage of each phase is reported in Table 1. Upon increasing the calcination temperature the percentage of anatase and rutile phases increase at the expense of brookite. The amount of anatase phase increases from 77 to 87% when the calcination temperature increases from 250 to 500 °C and the amount of rutile phase increases from 2 to 6%.

Nitrogen sorption isotherms revealed the presence of mesopores in the C,N-TiO_2 monolith skeletons characterized by sharp steps in the nitrogen isotherms (Figure 2b). By increasing the calcination temperature from 300 to 500 °C, the specific surface area decreases from 230 to 60 m^2/g, the mesopore volume decreases from 0.30 to 0.20 mL/g and the mesopore diameter increases from 7 to 12 nm (Table 2). The high specific surface areas (100-200 m^2/g for calcination temperatures of 300-400 °C) together with large mesopore diameters in hierarchical macro-/mesoporous materials are highly suitable for photocatalysis processes [41]. An opposite trend (lower specific surface area, lower mesopore volume) was observed for the monolith calcined at 250 °C in comparison to the one calcined at 300 °C due to some higher amount of carbon residues at the surface as shown below by TGA. The mesopores result from the voids between the TiO_2 nanoparticles aggregates. SEM pictures at low and high magnification have been performed (Figures 1, S1). The macroporous network does not change upon calcination, featuring macropores of 3 microns in size and a skeleton thickness of 1.5 micron (Figure 1). Inside the skeleton, the TiO_2 nanoparticles show a spherical morphology of 10 nm after calcination at 250 °C. After calcination at 300 to 400 °C a mixture of 10 nm spherical nanoparticles and 20 x 50 nm nanorods, and at 450-500 °C mainly rods are observed (Figure S1). Upon increasing temperature there is an aggregation of the spherical particles into rods, which are growing in size. The diameters of the rods are in accordance with the particle sizes derived from the surface area determined from nitrogen sorption isotherms (Table 2).

3.2. Optical properties of TiO_2 monoliths

Optical properties of TiO_2 monoliths treated at different temperatures have been examined by DRUV spectroscopy (Figure 3a). The goal was to identify their light absorption properties and their absorption threshold. Extremely high absorption in the visible light domain has been observed for TiO_2 monoliths calcined between 250 and 350 °C, resulting in very low energy gaps around 1.5 eV (Figure 3b). Energy gaps were calculated by converting the wavelength to the energy and drawing a linear fit of the decreasing curve, where the

intercept with the X-axis defines the energy gap [46]. In opposite, TiO_2 monoliths treated at 400 and 500 °C display the same absorbance in the UV domain, as commercial anatase and P25 benchmark materials, with an absorbance decreasing drastically between 350 and 400 nm and becoming zero between 450 and 500 nm (Figure 3a,c). This absorbance in UV light corresponds to an energy gap of 3.2 eV in accordance with the theoretical energy band gap of anatase (3.2 eV). Figure 3d conclusively shows that the decrease of the value of the energy gap correlates with the carbon and nitrogen contents of the samples.

The high visible light absorption in the wavelength range of 380-700 nm for TiO_2 monoliths calcined between 250 and 350 °C could have three origins (alone or mixed):

- the formation of Ti-C and Ti-N bonds in the TiO_2 network
- the grafting of the surface of TiO_2, forming Ti-O-C bonds (reaction with isopropanol and/or PEO) and Ti-N bonds (reaction with NMF).
- Absorption of visible light by carbon species adsorbed at the surface of titania (no chemical bonds).

In literature, N-doped TiO_2 materials made by reacting TiO_2 nanoparticles with urea and heated for 30 min at different temperatures from 300 to 500 °C, were showing an increasing absorption in visible light region when the temperature was increased with a band gap decrease to 2.11 eV after an heating treatment at 500 °C [47]. Furthermore, for TiO_2 nanoparticles treated with urea, the amount of N increases in the materials with the increase of temperature until 450 °C, certainly due to in-situ formation of ammonia, which is known to react with TiO_2 at 600 °C, and decrease for calcination at 500 °C, with an amount remaining higher than for a calcination at 350 °C. Therefore, these differences between urea treatment in literature (lower band gap narrowing, increasing amount of N with increase of temperature) with our TiO_2 monoliths formed in presence of NMF can, in a first approximation, exclude the sole N-doping mechanism by the reaction of TiO_2 monoliths with NMF, some carbon species have to be responsible for this high visible light absorption and higher band gap narrowing.

Thermogravimetric (TGA) measurements, elemental analysis (EA) and X-ray photoelectron spectroscopy (XPS) have been performed on TiO_2 monoliths to determine the amount and investigate the nature of C-based and N-based species present in the monoliths as doped-, grafted- or adsorbed-species.

TGA profiles reveal three types of behaviors as a function of the calcination temperature (Figure 4). On materials calcined at 250 °C, three domains of weight loss are clearly identified. A first one, between 20 and *ca* 230°C, corresponds to the desorption of

physisorbed water (*ca* 5 wt%) while two other weight losses, at 230-330°C and 330-450°C are due to the desorption of weakly (4 wt%) and more strongly (7.3 wt%) adsorbed organic species, respectively. On materials calcined at 300 and 350°C, two weight losses are observed, the one due to physisorbed water (4.5 wt%) and the high temperature desorption of organic at 330-450°C amounting to 6 and 4.5 wt%, respectively. Finally, on materials calcined above 400°C the weight loss occurs smoothly from ambient till 800°C, and correspond essentially to a dehydroxylation of the surface. These materials contain only trace amounts, if any, of organic matter, in line with their optical properties.

Chemical analysis (Table 1, Figure 3) data are in line with TGA measurements and reveal in addition that the organic material desorbed at high temperature features a molar C/N ratio of 3.5. This indicates that besides NMF (C/N = 2), several moieties, such as ethylene oxide and/or isopropyl alcohol are at the origin of the retained organics.

The incorporation of C and N in the TiO_2 monolith was also investigated by XPS spectroscopy (Figure 5).

On all monoliths, regardless of the calcination temperature, C1s spectra consist in three large peaks ascribed to C-C (285 eV), C-O (286.5 eV) and C=O (288.7 eV) bonds, respectively [46]. This signal results essentially from a contamination of the surface. No signal at 282 eV, which could indicate the presence of Ti-C bonding could be detected [24]. Similarly, the N 1s peak at 396 eV that is thought to evidence the presence of substitutional nitrogen [47] was not detected. A rather broad N 1s signal peak centered at 400 eV is observed, which can be ascribed to nitrogen species in a higher oxidation state, for example nitrogen species containing NC or NCO bonds [47] as in NMF (O=C(H)-NH-CH_3), most probably coming from the grafting of NMF at the surface of TiO_2 through Ti-N bonds. This N 1s peak may be also assigned to anionic N^- in N-Ti-O bonds [48] suggesting that NMF could be immobilized on the surface either via grafting by covalent bond or via strong electrostatic interactions.

O1s XPS survey spectra of monolith samples treated at various temperatures are shown in Fig. 5. Each spectrum exhibits two peaks: one at around 529.5 eV for the regular lattice oxygen (Ti-O-Ti) [49] and the other at about 532 eV, which is ascribed to the oxygen in Ti-O-C arrangements [50]. The latter peak supports the hypothesis of a grafting of carbon moieties at the surface of the TiO_2 network.

Monoliths calcined at 400-500 °C show Ti $2p_{3/2}$ peaks at 458.8 eV as expected for TiO_2 materials (459.0 eV) with a slight shift of 0.2 eV. For monoliths calcined at 250, 300 and 350 °C, larger shifts (0.9, 0.7 and 0.4 eV) are observed with Ti 2p peaks at 458.1, 458.3 and 458.6 eV, respectively. The shift to lower binding energies suggests that some Ti^{4+} atoms are

partially reduced to a lower oxidation state, presumably due to the nitrogen species bound to Ti as stated above. This shift indicates also a different electronic interaction of Ti with anions [48] as, in our case, Ti with deprotonated NMF^-. This shift has been also attributed to a higher amount of oxygen vacancies, which is not the case in the present study, as oxygen vacancies are observed for monoliths calcined above 400 °C with a atomic ratio O/Ti = 1.8, whereas monoliths calcined between 250 and 350 °C feature atomic O/Ti = 1.9-2.0 (Table 3). The oxygen vacancies for the monoliths calcined above 400 °C could be at the origin of the slight shift of 0.2 eV, but not for monoliths calcined between 250 and 350 °C. The shift observed for these materials is most probably due to the grafting of NMF at the surface of TiO_2 through Ti-N bonds. The decrease of grafted-NMF species at the surface of TiO_2 with the increase of calcination temperature leads to a lower shift of the peak. In literature, similar shifts of 0.5-0.7 eV have been observed for TiO_2 nanoparticles treated with urea at temperature above 400 °C [48].

In summary, nitrogen is introduced in the TiO_2 monoliths by grafting of NMF on the surface of TiO_2 through Ti-N bond (or strong electrostatic Ti^+ NMF^- bond) and carbon is introduced most probably by adsorption and grafting of PEO by strong H-bonding on Ti-OH surface sites, which lead to grafted ethylene oxide species through Ti-O-C bonds. Some carbon species could also result from the decomposition of isopropanol coming from $Ti(OiPr)_4$. The adsorbed and/or grafted carbonaceous species on the surface of the monoliths calcined between 250 and 350 °C can cause reduced reflection of light and may be another important factor for the photocatalytic activity. Carbons can absorb the electrons and promote the separation of the electrons and holes to maintain their high activity [48]. Oxygen vacancies acted as recombination centers for holes and electrons do not seem to exist for monoliths calcined from 250 to 350 °C. High specific surface area, high mesopore volume, large mesopore diameter are also important factors in catalysis to increase the access to the active sites. For photocatalytic experiments, the TiO_2 monoliths calcined at 350 °C have been chosen as the best compromise between high visible light absorption (400-700 nm), high surface area (160 m^2/g), large mesopores diameter (9 nm), high mesoporous volume (0.30 mL/g) and high amount of anatase (83%).

3.3. Orange G Dye photocatalytic degradation

Dyes are widely used for printing, food, cosmetic and clinical purposes as well as textile dyeing because of their chemical stability, ease of synthesis and versatility. Their stability, however, causes pollution once the dyes are released into the environment. More

than 800,000 tons of dyes are annually produced worldwide, of which 60 to 70 % are azo dyes. Some azo dyes are toxic and mutagenic and thus the elimination of these dyes is now of major scientific and technologic challenge [51]. Physico-chemical treatments (adsorption, coagulation/flocculation precipitation, etc.) are usually performed to process industrial effluents. In spite of their rapidity, these methods have turned out to be ineffective in attaining the required regulation standards. Biological [51] and photochemical processes [52] are receiving increasing interest owing to their cost effectiveness and their ability to produce less sludge. The use of photocatalytic processes under sunlight would avoid the use of UV-A or UV-C lights and afford more sustainable processes. In addition, monoliths would insure significant process intensification by operating under continuous flow, with no powders to handle and more safety. In this study Acid Orange G dye, (1,3-naphtalene disulfonic acid) has been chosen as dye model molecule (Figure 6). It is an organic molecule belonging to the class of di-azo dyes used in the production of colored inks, highlighters, plastics, papers and textiles. It is carcinogenic and mutagenic.

Figures 6, S2 and Table 4 highlight the ability of C,N-TiO_2 monoliths to degrade Orange G under natural sunlight as well as under artificial light. In batch mode, upon irradiation by natural light the solution of dye (80 mg/L) was almost totally discolored (99 % of dye elimination) after one hour exposure (Figure 6, Table 4). The contribution of adsorption in the pores and on the surface of the monolith in the degradation process is marginal, representing 12% maximum of the amount of dye eliminated. Under these conditions, P25 TiO_2 proved hardly efficient, allowing only 37% dye degradation after 10 hours exposure.

Similarly, under more dilute conditions (7.35 g/L instead of 25g/L of photocatalyst) and using the irradiation of a neon lamp, nearly 80% of the dye was degraded with C,N-TiO_2 monoliths after 90 minutes exposition whereas the commercial P25 was totally inactive (Figure S2).

Interestingly, the potential of C,N-TiO_2 monoliths to degrade the solution of dye under natural sunlight was demonstrated in continuous flow experiments using the monolith as self-supporting reactor. Figure 7 shows the variation of the concentration of Orange G as a function of time of a 50 mL solution containing initially 80 mg/L of dye recirculated with a rate of 2 mL/min through the photocatalyst at ambient temperature. After 30 minutes on stream, corresponding to *ca* one passage of the whole volume of solution over the monolith, 50% of the dye has been degraded. Complete degradation was achieved after 4 hours recirculation. The monolith could be reused without loss of activity.

4. Conclusions

C,N-self-grafted TiO_2 monoliths through Ti-N and Ti-O-C bonds featuring an homogeneous and interconnected network of macropores of 3 μm have been obtained with a skeleton thickness of 1.5 μm by combining spinodal decomposition with sol-gel transition under proper solvothermal and thermal treatments. The C,N-TiO_2 monoliths calcined at 350 °C exhibit the anatase crystalline structure with high specific surface area (160 m^2/g) and large mesopore diameters (9 nm). The light absorbance in the domain of visible light is remarkable leading to a band gap decrease from 3.2 eV for anatase to 1.5 eV for C,N-TiO_2 monoliths. High Orange G dye degradation rates have been obtained in photocatalysis process under natural sunlight and artificial visible light in batch, whereas no discoloration of the solution was observed with benchmark P25 TiO_2 nanoparticles. The C,N-TiO_2 monoliths have been used as self-standing reactors for in flow photocatalysis in a recirculation mode under natural sunlight demonstrating remarkable activity. C,N-TiO_2 monoliths appear at a new family of photocatalysts highly efficient under visible light and easy to handle. These materials are very promising for environmental remediation technology as photocatalytic purification of polluted air and wastewater, able to develop degradation of pollutants in batch with an easy separation or in continuous flow treatments processes. Moreover, the macroporous flow-through network can be shaped as films, tapes or membranes to optimize light harvesting and cope with the requirements of the process technology. Further studies are in progress to expand the domains of application and fully describe the photochemical properties of these materials.

ACKNOWLEDGMENTS

Authors thank TOTAL SA and CNRS for financial support, Dr Dan Lerner for his help in visible light experiments and Dr Zhu Yang for advices in phase separation. The authors wish to acknowledge the support from the Chemistry Plateform of Campus in Montpellier (Plateform MEA University Montpellier), on which SEM, EDS and XPS have been performed.

REFERENCES

1. N. Linares, S. Hartmann, A. Galarneau, P. Barbaro, ACS Catal. 2 (2012) 2194-2198.

2. A. Galarneau, A. Sachse, B. Said, C. H. Pelisson, P. Boscaro, N. Brun, L. Courtheoux, N. Olivi-Tran, B. Coasne, F. Fajula, F., C. R. Chimie 19 (2016) 231-247.

3. A. Galarneau, Z. Abid, B. Said, Y. Didi, K. Szymanska, A. Jarzebski, F. Tancret, H. Hamaizi, A. Bengueddach, F. Di Renzo, F. Fajula, Inorganics 4 (2016) 9

4. U. I. Gaya, A. H. Abdullah, J. Photochem. Photobiol. C: Photochem. Rev. 9 (2008) 1-12.

5. C. M. Teh, A. R. Mohamed, J. Alloys Comp. 509 (2011) 1648-1660.

6. M. Pelaez, N. T. Nolan, S. C. Pillai, M. K. Seery, P. Falaras, A. G. Kontos, P. S. M. Dunlop, J. W. J. Hamilton, J. A. Byrne, K. O'Shea, M. H. Entezari, D. D. Dionysiou, Appl. Catal. B. Environ. 125 (2012) 331-349.

7. K. Nakata, A. Fujishima, J. Photochem. Photobiol. C: Photochem. Rev. 13 (2012) 169-189.

8. Y. Wang, Y. He, Q. Lai, M. Fan, J. Env. Sci. 26 (2014) 2139-2177.

9. S. Banerjee, S. C. Pillai, P. Falaras, K. E. O'Shea, J. A. Byrne, D. D. Dionysiou, J. Phys. Chem. Lett. 5 (2014) 2543-2554.

10. V. Etacheri, C. Di Valentin, J. Schneider, D. Bahnemann, S. C. Pillai, J. Photochem. Photobiol. C: Photochem. Rev. 25 (2015) 1-29.

11. J. Schneider, M. Matsuoka, M. Takeuchi, J. Zhang, Y. Horiuchi, M. Anpo, D.W. Bahnemann, Chem. Rev. 114 (2014) 9919−9986.

12. S. Gunti, A. Kumar, M. K. Ram, Int. Mater. Rev. 63 (2018) 257-282.

13. P. Mazierski, A. Mikolajczyk, B. Bajorowicz, A. Malankowska, A. Zaleska-Medynska, J. Nadolna, Appl. Catal. B: Environ. 233 (2018) 301-317.

14. A. E. Giannakas, M. Antonopoulou, C. Daikopoulos, Y. Deligiannakis, Appl. Catal. B: Environ. 184 (2016) 44-54.

15. W. Wang, M.O. Tadé, Z. Shao, Prog. Mater. Sci. 92 (2018) 33–63.

16. G. Barolo, S. Livraghi, M. Chiesa, M.C. Paganini, E. Giamello, J. Phys. Chem. C. 116 (2012) 20887-20894.

17. R. Asahi, T. Morikawa, H. Irie, T. Ohwaki, Chem. Rev. 114 (2014) 9824–9852.

18. R. Leary, A. Westwood, Carbon 49 (2011) 741–772.

19. N. R. Khalid, A. Majid, M. B. Tahir, N. A. Niaz, S. Khalid, Ceramics Int. 43 (2017) 14552–14571.

20. W. Ren, Z. Ai, F. Jia, L. Zhang, X. Fan, Z. Zou, Appl. Catal. B. Environ. 69 (2007) 138-144.

21. F. Dong, S. Guo, H. Wang, X. Li, Z. Wu, J. Phys. Chem. C. 115 (2011) 13285-13292.

22. Z. Barbierikova, E. Plizingrova, M. Motlochova, P. Bezdicka, J. Bohacek, D. Dvoranova, M. Mazur, J. Kupcik, J. Jirkovsky, J. Subrt, J. Krysa, V. Brezova, Appl. Catal. B: Environ. 232 (2018) 397-408.
23. C. Cheng, X. Tan, D. Lu, L. Wang, T. Sen, J. Lei, A. M. El-Toni, J. Zhang, F. Zhang, D. Zhao, Chem. Eur. J. 21 (2015) 17944-17950.
24. M. A. Mohamed, J. Jaafar, M. F. M. Zain, L. J. Minggu, M.B. Kassim, M. S. Rosmi, N. H. Alias, N. A. M. Nor, W. N. W. Salleh, N.H.D. Othman, Appl. Surf. Sci. 436 (2018) 302-318.
25. T. Jia, F. Fua, D. Yua, J. Caob, G. Sunb, Appl. Surf. Sci. 430 (2018) 438-447.
26. D. Wang, L. Jia, X. Wu, L. Lu, A. Xu, Nanoscale, 4 (2012) 576-584.
27. M. Triantis, T. Fotiou, T. Kaloudis, A. G. Kontos, P. Falaras, D. D. Dionysiou, M. Pelaez, A. Hiskia, J. Hazard. Mater. 211 (2012) 196-202.
28. Y. Zhang, Z. Zhao, J. Chen, L. Cheng, J. Chang, W. Sheng, C. Hu, S. Cao, Appl. Catal. B. Environ. 165 (2015) 715-722.
29. V. Hulea, E. Dumitriu, Nano-oxides, in Nanomaterials in Catalysis. P. Serp, K. Philippot (eds), Wiley-VCH, Weinheim, 2013, pp. 375-413.
30. D. L. Liao, B. Q. Liao, J. Photochem. Photobiol. A: Chem. 187 (2007) 363-369.
31. J. Chen, F. Qiu, W. Xu, S. Cao, H. Zhu, App. Catal. A. 495 (2015) 131-140
32. L. N. Quan, Y. H. Jang, K. A. Stoerzinger, K. J. May, Y. J. Jang, S. T. Kochuveedu, Y. Shao-Horn, D. H. Kim, Phys. Chem. Chem. Phys. 16 (2014) 9023-9030.
33. Chen, T. L. Zhang, J. Fan, D. B. Kuang, C. Y. Su, ACS Appl. Mater. Interfaces, 5 (2013) 9205-9211.
34. S. Linley, T. Leshuk, F. X. Gu, ACS Appl. Mater. Interfaces, 5 (2013) 2540-2548.
35. M. C. Orilall, N. M. Abrams, J. Lee, F. J. Di Salvo, U. Wiesner, J. Am. Chem. Soc. 130, 28 (2008) 8882-8883.
36. T. Kamegawa, D. Yamahana, H. Yamashita, J. Phys. Chem. C. 114 (2010) 15049-15053.
37. S. Takenaka, T. Arike, H. Matsune, M. Kishida, Appl. Catal. B: Environ. 125 (2012) 358-366.
38. D. Zhao, X. Yang, C. Chen, X. Wang, J. Colloid Interface Sci. 398 (2013) 234-239.
39. X. Li, W. Zhang, H. Pan, Y. Yu, L. Chen, P. Wu, J. Catal. 300 (2013) 9-19.
40. Kouame, N. A.; Robert, D.; Keller, V.; Keller, N.; Pham, C.; Nguyen, P. Env. Sci. Pollution Research. 19 (2012) 3727-3734.
41. J. G. Yu, Y. R. Su, B. Cheng, Adv. Funct. Mater. 17 (2007) 1984-1990.
42. J. Konishi, K. Fujita, K. Nakanishi, K. Hirao, Chem. Mater. 18 (2006) 6069-6074.

43. J. Konishi, K. Fujita, K. Nakanishi, K. Hirao, K. Morisato, S. Miyazaki, M. Ohira, J. Chrom. A, 1216 (2009) 7375-7383.
44. K. Thamaphat, P. Limsuwan, B. Ngotawornchai, Kasetsart J. (Nat. Sci.) 42 (2008) 357-361.
45. A. Galarneau, D. Desplantier, R. Dutartre, F. Di Renzo, Microporous Mesoporous Mater. 27 (1999) 297-308.
46. F. Dong, H. Wang, Z. Wu, J. Phys. Chem. C 113 (2009) 16717-16723.
47. R. Beranek, H. Kisch, Photochem. Photobiol. Sci. 7 (2008) 40-48.
48. X. Liu, Y. Chen, C. Cao, J. Xu, Q. Qian, Y. Luo, H. Xue, L. Xiao, Y. Chen, Q. Chen, New J. Chem., 39 (2015) 6944-6950.
49. Y. Park, W. Kim, H. Park, T. Tachikawa, T. Majima, W. Choi, Appl. Catal. B: Environ. 91 (2009) 355-361.
50. C. Cheng, D. Lu, B. Shen, Y. Liu, J. Lei, L. Wang, J. Zhang, M. Matsuoka, Microporous Mesoporous Mater. 226 (2016) 79-87.
51. H. B. Mansour, O. Boughzala, D. Dridi, D. Barillier, L. Chekir-Ghedira, R. J. Mosrati, Water Sci. 24 (2011) 209-238.
52. W. Wei, C. Yu, Q. Zhao, G. Li, Y. Wan, Chem. Eur. J. 19 (2013) 566-577.

Figures captions

Figure 1. Schematic representation of the synthesis protocol of the C,N-TiO_2 monoliths. Picture and SEM image of C,N-TiO_2 monolith

Figure 2. (a) XRD patterns and (b) nitrogen sorption isotherms at -196 °C of C,N-TiO_2 monoliths calcined at different temperatures.

Figure 3. (a) Absorbance spectra (calculated via the Kubelka-Munk transformation) of (a) C,N-TiO_2 monoliths treated at different temperatures between 250 and 500 °C with the corresponding (b) calculated energy gaps, (d) C, N composition and (e) of commercial anatase benchmark material and P25.

Figure 4. Thermogravimetric analysis of C,N-TiO_2 monoliths treated at different temperatures between 250 and 500 °C.

Figure 5. Ti 2p, O 1s, N 1s, C 1s XPS spectra for C,N-TiO_2 monoliths treated at various temperatures between 250 and 500 °C.

Figure 6. Orange G dye formula and pictures of the supernatant solutions resulting from the photodegradation of Orange G dye solution (80 mg/L) in batch under natural sunlight as a function of time using pieces of C,N-TiO_2 monolith (25 g/L) treated at 350 °C. Comparison with benchmark TiO_2 P25 nanoparticles and native solution free of catalyst (Blank).

Figure 7. Elimination of Orange G (50 mL of solution at 80 mg/L) with C,N-TiO_2 monolith as a function of time of exposure to natural sunlight under recirculation flow mode (2 mL/min).

Table 1. Carbon and nitrogen content and phase composition of C,N-TiO_2 monoliths as a function of calcination temperature.

T (°C)	C (wt%)	N (wt%)	Anatase (%)	Brookite (%)	Rutile (%)
250	4.0	1.2	76.8	21.0	2.2
300	3.0	1.0	78.8	18.8	2.4
350	1.5	0.5	83.4	12.7	3.9
400	0.15	0.05	86.9	7.7	5.4
450	0.1	0.03	87.4	6.8	5.8
500	0.02	0.02	86.9	6.9	6.2

Table 2. Textural features of C,N-TiO_2 monoliths determined by nitrogen sorption at -196 °C as a function of calcination temperature: specific surface area (S_{BET}), mesoporous volume (V), mesopore diameter (D), particle diameter (6/ρS,) with ρ= 3.893 g/cm^3 (anatase).

T (°C)	S_{BET} (m^2/g)	V (mL/g)	D (nm)	Particle diameter 6/ρS (nm)
250	188	0.24	6.5	8.2
300	228	0.30	7.0	6.7
350	155	0.30	8.6	9.9
400	98	0.23	9.9	15.7
450	82	0.23	11.0	18.8
500	65	0.20	11.8	23.7

Table 3. Atomic O, Ti contents in C,N-TiO_2 monoliths calcined at different temperatures from 250 to 500°C determined by XPS.

T (°C)	O 1s (at%)	Ti 2p (at%)	O/Ti
250	43.23	21.53	2.01
300	46.85	24.65	1.90
350	45.89	23.75	1.93
400	48.95	27.16	1.80
450	48.49	27.42	1.77
500	46.95	26.15	1.79

Table 4. Concentration of dye as a function of time in batch experiments under natural sunlight exposure with pieces of TiO_2 monoliths calcined at 350 °C. Comparison with benchmark TiO_2 nanoparticles P25, blank and adsorption in the dark.

Sample	Concentration of orange G (mg/L)		
Exposure time	1 h	5 h	10 h
Blank	80 ± 0.1	79.9 ± 0.1	81 ± 0.1
Monolith not exposed to light	72 ± 4	79 ± 5	70 ± 3
P25 TiO_2	76 ± 2	67 ± 6	51 ± 3
Monolith	0.36 ± 0.06	0.08 ± 0.08	0.08 ± 0.07

Figure 1

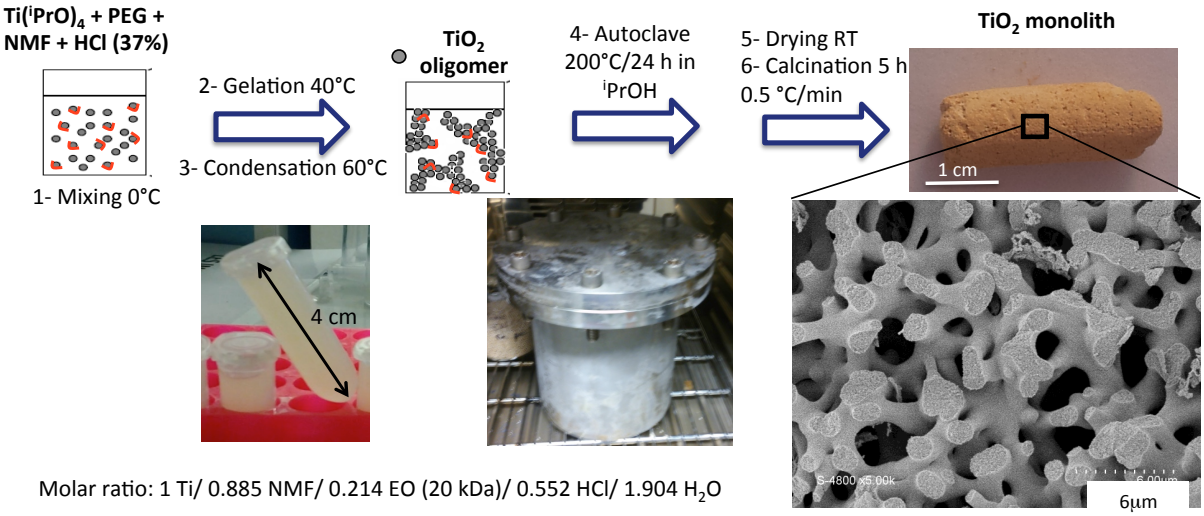

Molar ratio: 1 Ti/ 0.885 NMF/ 0.214 EO (20 kDa)/ 0.552 HCl/ 1.904 H_2O

Figure 2

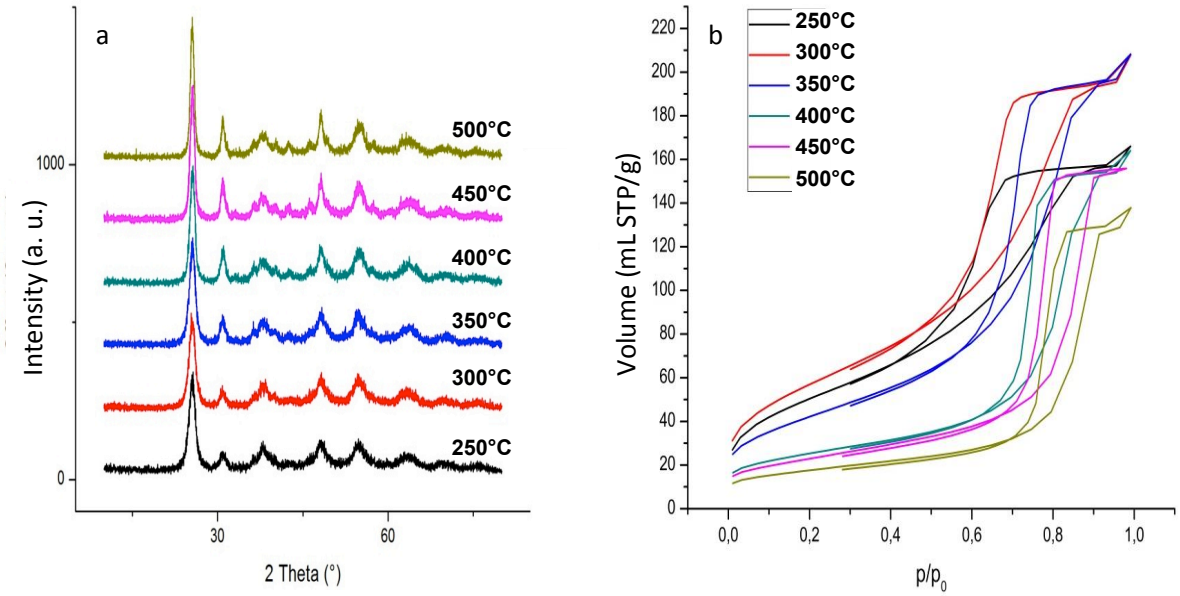
a
500°C
450°C
400°C
350°C
300°C
250°C
Intensity (a. u.)
1000
0
30
60
2 Theta (°)
b
250°C
300°C
350°C
400°C
450°C
500°C
Volume (mL STP/g)
220
200
180
160
140
120
100
80
60
40
20
0
0,0
0,2
0,4
0,6
0,8
1,0
p/p0

Figure 3

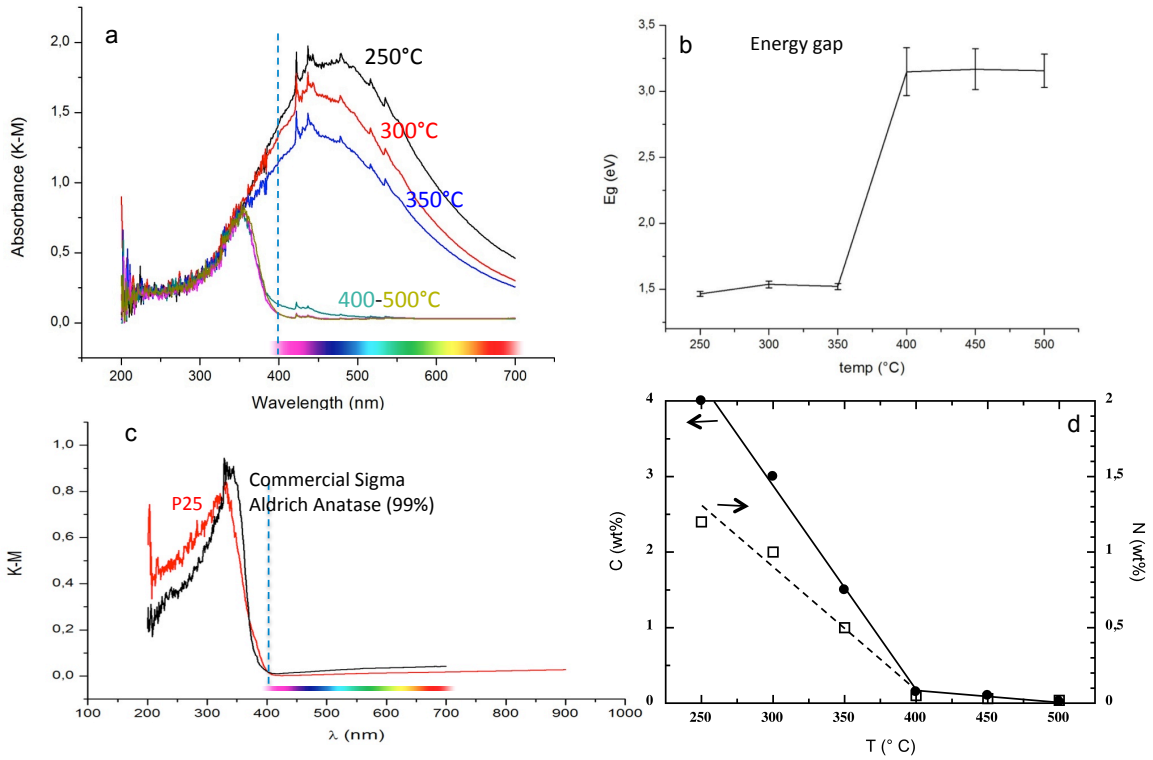
a
250°C
300°C
350°C
400-500°C
Absorbance (K-M)
Wavelength (nm)
b
Energy gap
Eg (eV)
temp (°C)
c
P25
Commercial Sigma
Aldrich Anatase (99%)
K-M
λ (nm)
d
C (wt%)
N (wt%)
T (° C)

Figure 4

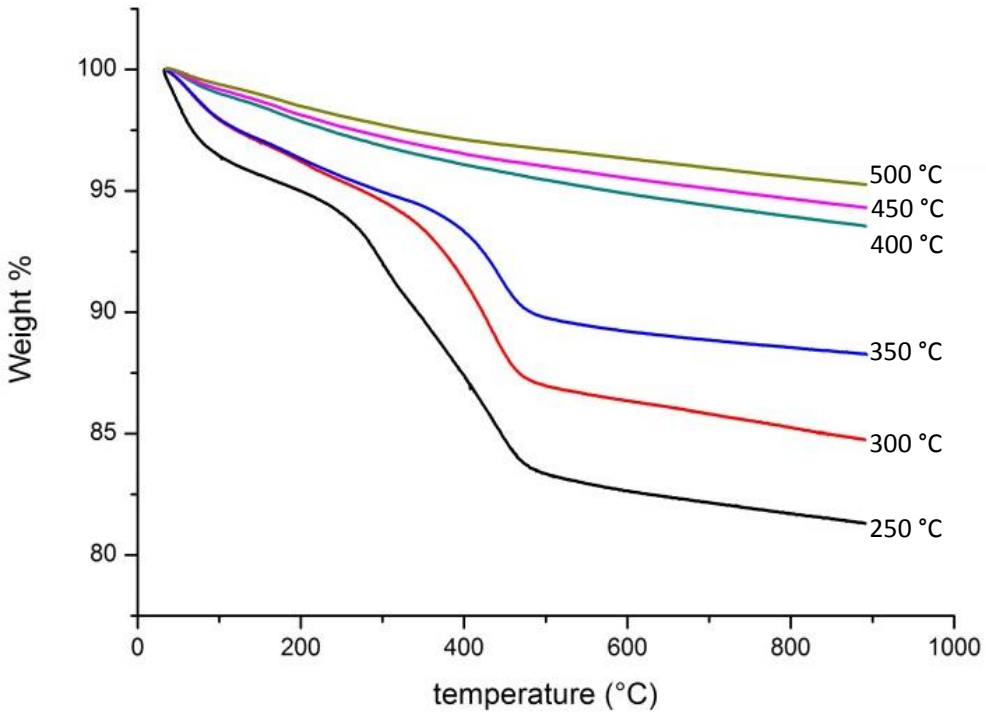
100
95
90
85
80
Weight %
0
200
400
600
800
1000
temperature (°C)
500 °C
450 °C
400 °C
350 °C
300 °C
250 °C

Figure 5

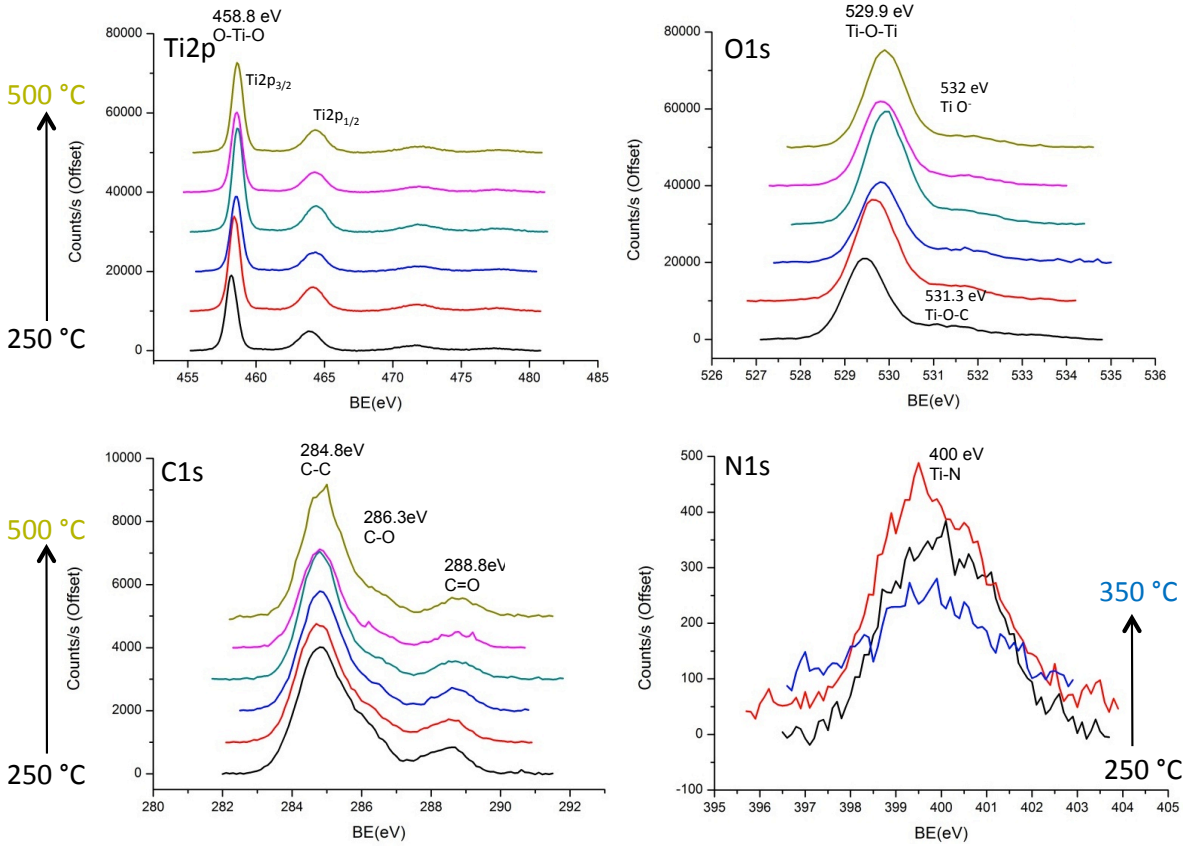
Ti2p
458.8 eV
O-Ti-O
Ti2p3/2
Ti2p1/2
500 °C
250 °C
Counts/s (Offset)
BE(eV)
O1s
529.9 eV
Ti-O-Ti
532 eV
Ti O-
531.3 eV
Ti-O-C
C1s
284.8eV
C-C
286.3eV
C-O
288.8eV
C=O
N1s
400 eV
Ti-N
350 °C
250 °C

Figure 6

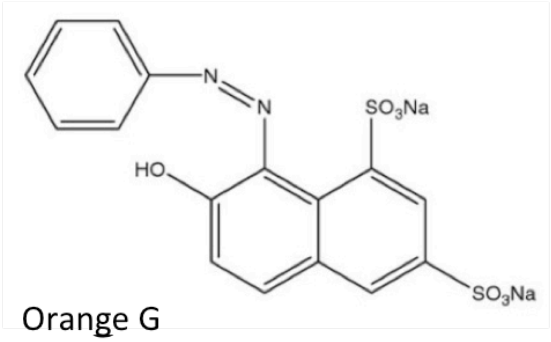

Orange G

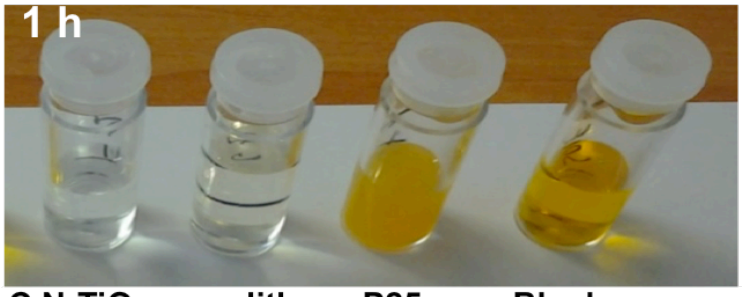

C,N-TiO_2 monoliths P25 Blank

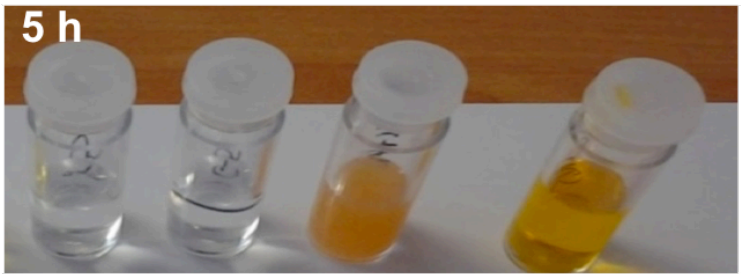

C,N-TiO_2 monoliths P25 Blank

C,N-TiO_2 monoliths P25 Blank

Figure 7

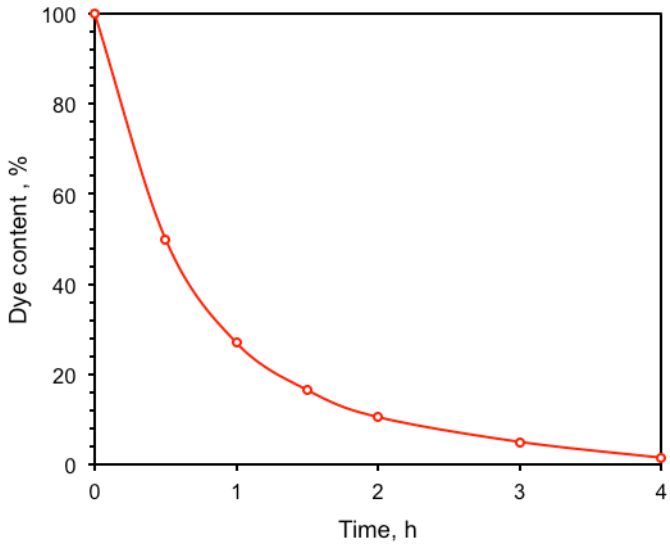

Graphical Abstract